The Astrophysical Journal Letters, 929:L10 (7pp), 2022 April 10 https://doi.org/10.3847/2041-8213/ac62d4

Magnetic Switchback Occurrence Rates in the Inner Heliosphere: Parker Solar Probe and 1 au

Francesco Pecora[1], William H. Matthaeus[1], Leonardo Primavera[2], Antonella Greco[2], Rohit Chhiber[1,3], Riddhi Bandyopadhyay[4], and Sergio Servidio[2]
[1] Department of Physics and Astronomy, University of Delaware Newark, DE 19716, USA; fpecora@udel.edu
[2] Dipartimento di Fisica, Università della Calabria, 87036 Arcavacata di Rende, Italia
[3] Heliophysics Science Division, NASA Goddard Space Flight Center, Greenbelt, MD 20771, USA
[4] Department of Astrophysical Sciences, Princeton University Princeton, NJ 08544, USA
Received 2022 February 4; revised 2022 March 30; accepted 2022 March 31; published 2022 April 11

Abstract

The subject of switchbacks, defined either as large angular deflections or polarity reversals of the magnetic field, has generated substantial interest in the space physics community since the launch of the Parker Solar Probe (PSP) in 2018. Previous studies have characterized switchbacks in several different ways and have been restricted to data available from the first few orbits. Here, we analyze the frequency of occurrence of switchbacks per unit distance for the first full eight orbits of PSP. In this work, events that reverse the sign of the magnetic field relative to a regional average are considered switchbacks. A significant finding is that the rate of occurrence falls off sharply approaching the Sun near 0.2 au (40 $R_{\odot}$) and rises gently from 0.2 au outward. The analysis is varied for different magnetic field cadences and for different local averages of the ambient field, confirming the robustness of the results. We discuss implications for the mechanisms of switchback generation. A publicly available database has been created with the identified reversals.

Unified Astronomy Thesaurus concepts: Interplanetary magnetic fields (824); Interplanetary medium (825); Interplanetary turbulence (830)

1. Introduction

The orbit of the Parker Solar Probe (PSP) has taken the mission into previously unexplored regions of the heliosphere in which both new phenomena, related to the origin of the solar wind, and known ones, from a rather different perspective, can be observed (Fox et al. 2016). The phenomenon of magnetic field "switchbacks" (SBs), defined either as large deflections or polarity reversals relative to ambient conditions, has been previously observed at larger distances (Borovsky 2016; Horbury et al. 2018), but it is more evident in the PSP environment close to the Sun.

A number of studies prior to PSP had already noted the existence of SBs in the interplanetary magnetic field (McCracken & Ness 1966; Neugebauer & Goldstein 2013; Borovsky 2016; Horbury et al. 2018). The origin of these SBs or "folds" has usually been discussed in association with phenomena closer to the Sun, such as interchange reconnection (Fisk & Kasper 2020; Schwadron & McComas 2021; Bale et al. 2021) or some form of local dynamical activity (e.g., Ruffolo et al. 2020; Squire et al. 2020). Generally, polarity reversals at the heliospheric current sheet (HCS) have been treated as a separate class.

Recently, numerous studies have examined detailed properties of SBs in PSP data (Horbury et al. 2020; McManus et al. 2020; Mozer et al. 2020; Laker et al. 2021; Mozer et al. 2021; Tenerani et al. 2021), while other studies have provided insight into both the possible origin of SBs (Landi et al. 2006) and their propagation and dissipation (Tenerani et al. 2020; Magyar et al. 2021a, 2021b).

The purpose here is to provide a more complete perspective of the occurrence rates of SBs by employing the data from the initial eight orbits of PSP in a unified analysis. For specificity, we will consider strong SBs that reverse the local polarity of the magnetic field, corresponding to deflection angles greater than 90°.

The paper is organized as follows: Criteria for data selection and the definition of SBs are given in Section 2, the statistics of SB waiting times (WTs) and duration are presented in Section 3, the radial occurrence of SBs throughout the inner heliosphere is shown in Section 4, and the last section is dedicated to the discussion of the results. Finally, in the Appendix, the SB database is presented.

2. Data Selection and Switchback Identification

We use publicly available measurements of the magnetic field from the MAG instrument on the FIELDS (Bale et al. 2016) and the solar wind ion speed from SPC on the SWEAP (Kasper et al. 2016) suites on the PSP (Fox et al. 2016) during its first eight orbits. The analysis, from 2018 August 12 through 2021 June 19, is carried over nonoverlapping 6 hr-long intervals as suggested in Dudok de Wit et al. 2020 and Bandyopadhyay et al. 2021. The following procedure has been automated using the Python library AI.CDAS, which provides access to the CDAS database through the CDAS REST API. The API service provided by CDAS is an advantageous tool that allows a user to request data from the server and work with them dynamically. A 6 hr interval is considered for the analysis only if, when divided into six 1 hr-long subintervals, each subinterval has less than ∼30% of points missing. In that case, linear interpolation is performed to restore data continuity (if any missing point is present). Intervals with more than ∼30% of points missing were discarded. The same criterion has been

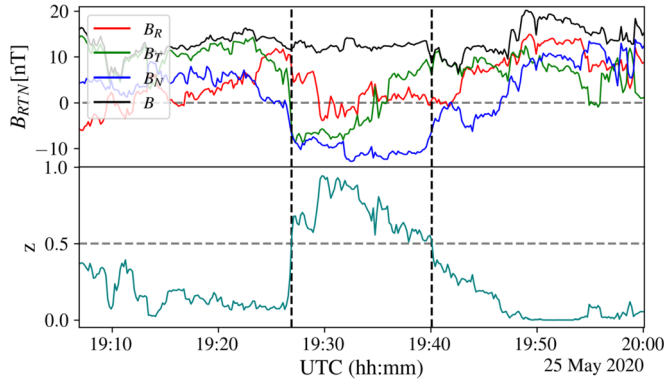

Figure 1. Example of a PSP time interval containing an SB, as defined in Equation (1) and by Dudok de Wit et al. (2020). (Top panel) Magnetic field measurements at 10 s resolution. (Bottom panel) The SB, delimited by the two vertical dashed lines, is identified in the interval where $z \geqslant 0.5$ and extends for ∼13 minutes.

used to skim Wind measurements, over the same period, for the magnetic field (MFI; Lepping et al. 1995) and bulk speed (SWE; Ogilvie et al. 1995). The detection of SBs was carried out using magnetic field measurements at 10 s and 60 s resolutions. To ensure that the choice of the above settings does not affect the results, the analyses have been repeated by changing the interval length to 3 hr and choosing a stricter limit of 15% of points missing per subinterval. We find a general consistency of results for the above variations of parameters. Therefore, the following analyses have utilized an interval duration of 6 hr and a ∼30% threshold in order to retain more intervals and a larger number of events.

The presence of SBs in each 6 hr interval is revealed using the "normalized deflection" measure z as defined by Dudok de Wit et al. (2020):

$$z = \frac{1}{2}[1 - \cos(\alpha)], \tag{1}$$

where α is the angle between the pointwise magnetic field $\boldsymbol{B}$ and a local average $\langle \boldsymbol{B} \rangle$ evaluated over the considered 6 hr. "Switchbacked" regions are those with a value of $z \geqslant 0.5$, corresponding to magnetic field deflections larger than 90° with respect to the local average. This is the main criterion employed in this study to define an SB. This seems to us to be less arbitrary than a choice of other thresholds for z that indicate nonreversing deflections.

Figure 1 shows an example of a detected SB using PSP magnetic field data at 10 s resolution. The z parameter is constantly above the selected threshold of 0.5 for ∼13 minutes. Notice that the reversal, using the definition given by Equation (1) (as in Dudok de Wit et al. 2020), is identified using the total magnetic field vector and is not only one component.

3. Waiting Times and Duration

The evaluation of the WT between two consecutive SBs and the duration of each event can provide insight into two fundamental questions: (I) do SBs tend to cluster, or are they more likely to be isolated events? (II) How do the WTs and durations of SBs relate to turbulence scales, i.e., integral and inertial range scales? These questions address the issue of whether SBs are part of the evolving solar wind.

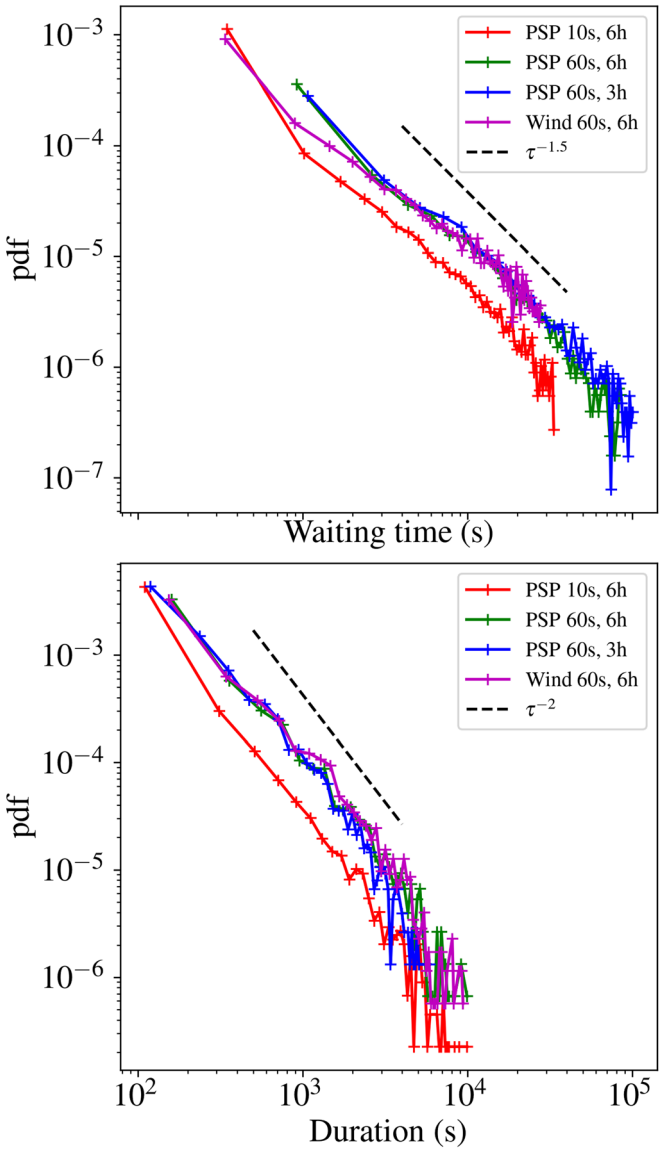

Figure 2. Distributions of (top) waiting times and (bottom) SB durations for the different tunable parameters—magnetic field time resolution and averaging window extension—used for PSP and for Wind. Dashed lines are reference slopes.

We define the duration of an SB as the number of consecutive above-threshold points times the cadence of magnetic field measurements employed (by this definition, a one-point SB lasts 10 s or 60 s depending on the data set used). In Figure 1, the duration of ∼13 minutes is given by all the consecutive above-threshold events within the vertical dashed lines. Instead, the WT between SBs is defined as the time elapsed between the end of an SB and the beginning of the following SB. This last measure is necessarily affected by the presence of missing data intervals. To avoid spurious too-long WTs, we discard WTs with values greater than $\mu + 3\sigma$, where μ is the mean of all the WTs and σ is the standard deviation. Figure 2 shows the distribution of WTs and duration for the different settings used to analyze PSP and Wind data, along with a reference slope.

Meaningful differences and similarities are evident in the distributions reported in Figure 2. With respect to the magnetic field resolution, all those obtained with a 60 s magnetic field

Table 1
Switchback Average Duration ($\langle\tau_{SB}\rangle$) and Waiting Times ($\langle\tau_{WT}\rangle$), Evaluated over the Period of 2018 August 12 through 2021 June 19 by Varying the Spacecraft (SC), the Magnetic Field Resolution (Δt), and the Averaging Window Width (W)

SC	Δt (s)	W (h)	$\langle\tau_{SB}\rangle$ (s)	$\langle\tau_{WT}\rangle$ (s)	$\langle\tau_{WT}\rangle$ (min)
PSP	60	6	450	4000	66
PSP	60	3	370	5500	91
PSP	10	6	200	1100	18
Wind	60	6	503	2600	43

overlap quite well. As will be discussed below, the only difference appears in the Wind WT distribution. The act of modifying the averaging window between 3 or 6 hr does not produce any appreciable variation. Instead, using different magnetic field cadences appears to be associated with appreciable changes in the distribution of WTs.

The distribution of SB durations shows a power-law tail with a slope approaching −2. Therefore, an average duration can be estimated as $\langle\tau_{SB}\rangle = \int_0^\infty t\ \mathrm{pdf}(t)\ dt$, which varies between 200 and 500 s. WT distributions, instead, show a slope closer to −1.5, for which the formal definition of an average WT is an ill-posed measure (Newman 2005). However, because the distributions have a finite extension, an approximate (population) average WT, ranging from 18 to 90 minutes, can be calculated with the available measurements.

Table 1 shows a summary of the above-mentioned results and parameters used for the analysis. Different columns list the spacecraft name, the magnetic field cadence, the width of the window, the average SB duration, and the average SB WT.

The distribution of WTs obtained with Wind measurements anticipates results to be discussed further in the next section. The maximum WT observed within all Wind measurements is much lower than the average WT observed with PSP using the same-cadence magnetic field (but also for higher cadence). Therefore, we can infer that SBs are more common at 1 au because the average WT is shorter.

Consistent with previous discussions of SBs (Dudok de Wit et al. 2020) and discontinuities as measured by the partial variance of increments (PVI) (Chhiber et al. 2020; Bandyopadhyay et al. 2020; Sioulas et al. 2022), we note that a power-law WT distribution is suggestive of clustering. That is, these distributions imply the presence of a correlation between successive SBs.

4. Radial Occurrence of Switchbacks

Early reports on SBs focused on PSP perihelia (Dudok de Wit et al. 2020; Mozer et al. 2020) and analyzed the first several orbits with somewhat contrasting selection criteria and correspondingly diverse results (Farrell et al. 2020; Mozer et al. 2021; Tenerani et al. 2021). With the release of the data from PSP orbit 8, the pool of available measurements spans about three years (one-third of the total nominal mission duration), and the study of the radial evolution of SBs becomes more accessible and statistically relevant.

More recent studies (Dudok de Wit et al. 2020; Liang et al. 2021; Martinović et al. 2021) also report surveys and vary rather significantly in both methodology and criteria for

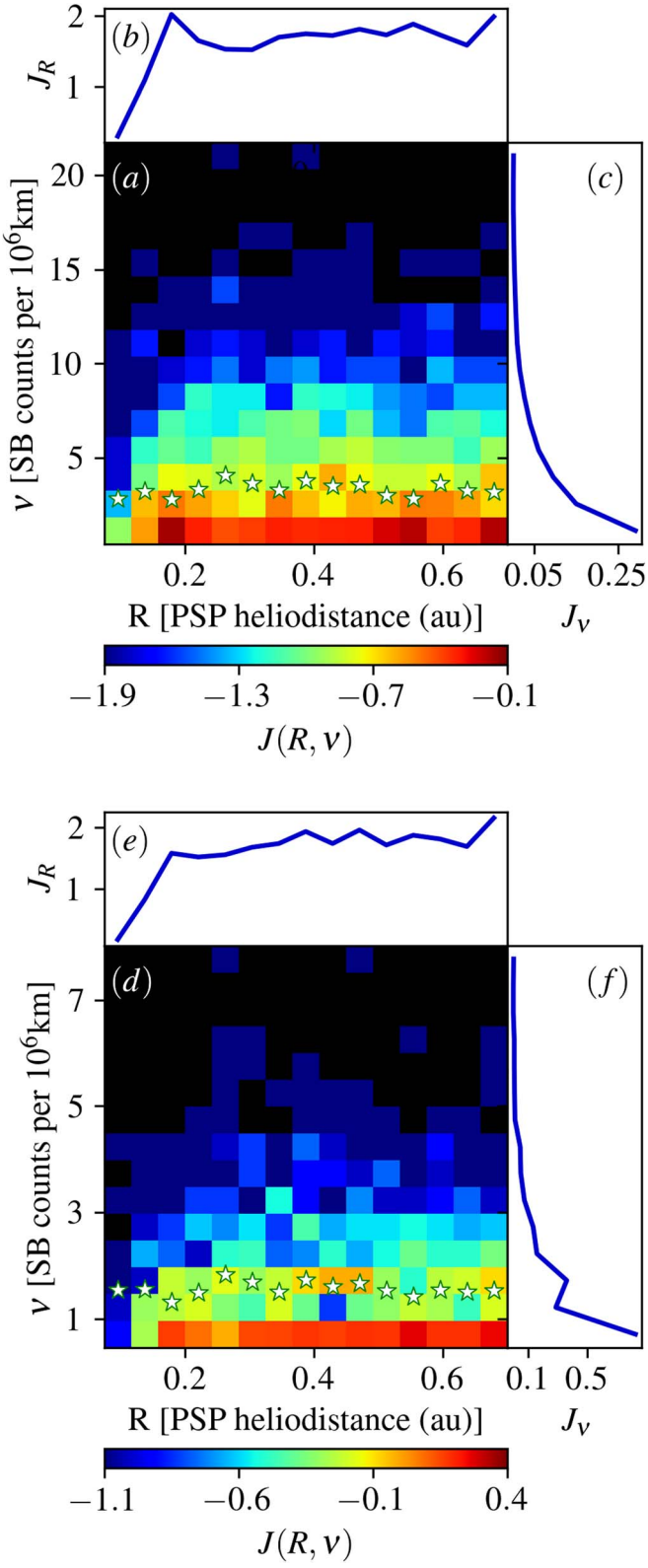

Figure 3. (Color plot) joint distribution $J(R, \nu)$ of SB counts per 10^6 km (ν) vs. PSP heliodistance (R), using the magnetic field at 10 s (a) and 60 s (d). Colors represent the probability distribution in log scale (black domains are regions with zero counts). The marginal probability distributions (see text) are shown in panels (b) and (c) for the 10 s and (e) and (f) for 60 s magnetic field. White stars represent the average value $\langle\nu\rangle$ for each column, i.e., $\langle\nu\rangle = \frac{\int d\nu' \nu' F(\nu', R^*)}{\int d\nu' F(\nu', R^*)}$.

selecting events. To date, the origin of SBs remains a matter of debate.

Figure 3 shows a principal result of the present study—the joint distributions of the occurrence of magnetic SBs per 10^6 km versus PSP radial distance. The population in each bin is determined as follows: After having identified all the SBs as discussed in Section 2, we count how many SBs occur in each one-hour long interval, and record the radial distance of PSP at that time. As one would expect, the occurrence of SBs would depend on the speed of the solar wind. We make use of the Taylor hypothesis (Jokipii 1973; Chhiber et al. 2019; Perez et al. 2021) to convert each one-hour interval to a spatial interval employing hourly averaged measurements of the solar wind bulk speed from SWEAP and SWE (for PSP and Wind, respectively). This estimate of SBs per unit length is tallied in the bins labeled by SBs per length versus heliocentric distance. Using the number of SBs per unit distance, which basically is a density of SBs, helps reduce the possible effects of PSP dwell time at different heliocentric distances, which otherwise might bias results based only on the total number of SB counts.

The rates are tabulated from all available data and are sorted in the binned parameter space (R, ν), where R is the PSP radial distance and ν is the number of SBs per Mkm. When this has been accumulated over the entire population, we obtained the joint distributions $J(R, \nu)$ that are shown in the color plots in panels (a) and (d) of Figure 3. The color parameter is a measure of the logarithm of the probability density in a particular cell of the (R, ν) grid. An immediate impression is that a lower rate of SBs per kilometer is found at the smallest heliodistances.

A more direct view of the occurrence can be recovered via the marginal distributions that are obtained from the joint probability density function (pdf). One marginal distribution is obtained by integration of the joint distribution over all radial distances, $J_\nu = \int J(R, \nu) dR$. This is the distribution of SB counts per Mkm without regard to the radial distance.

For the distribution computed from the 60 s data, noting the strong peak in J_ν in the range of $1 < \nu < 2$, one draws a "trivial" interpretation that it is more common to find one or two SBs per Mkm than it is to find several. A more physical interpretation of this result becomes apparent when recalling that the mean value of correlation lengths in the solar wind in the inner heliosphere gradually increases from about 500,000 km to 1,000,000 km from 0.16 au to 1 au (Ruiz et al. 2014; Chhiber et al. 2021; M. E. Cuesta et al. 2022, in preparation). Therefore, a simple interpretation of the substantial peaking of J_ν at values less than 2 for 60 s magnetic field data is that, averaged over the aggregate population within 1 au, SBs are found in the solar wind about once per correlation length. When 10 s data are used in the calculation, the marginal distribution J_ν retains a similar shape though stretched to a range of about $1 < \nu < 6$. This is consistent with the intuition that higher-time-resolution data can (and will) detect shorter time duration SBs that the coarser-resolution data cannot detect.

The other interesting marginal distribution is $J_R = \int J(R, \nu) d\nu$, that is, the distribution of SBs per radial distance, as a function of the radial distance, and integrated over all possible local occurrence rates. This marginal distribution displays two distinct regimes: (I) Descending below 0.2 au ($\sim 40\, R_\odot$), there is a sharp decrease in high SB count rates, and (II) a plateau is reached between 0.2 and 0.7 au (The available data from PSP at distances beyond 0.7 au are insufficient).

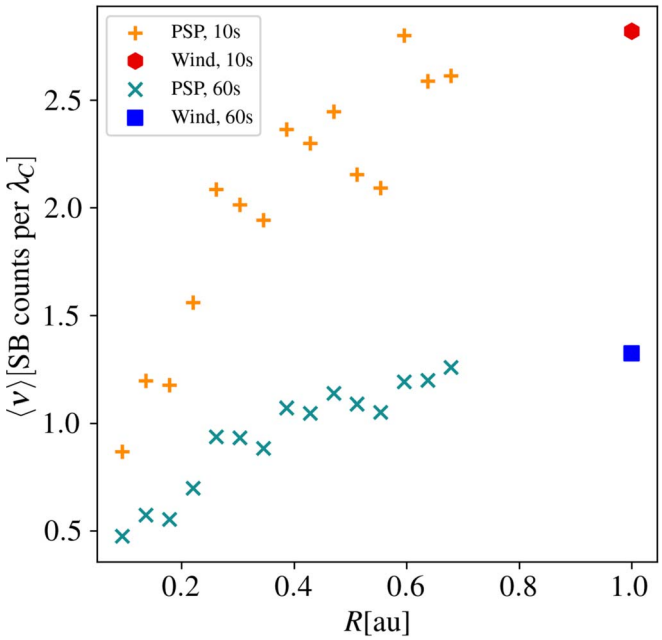

Figure 4. Average number of SBs per correlation length (estimated as $\lambda_C \sim 10^6\,\mathrm{km}\sqrt{R(\mathrm{au})}$), as a function of the heliodistance.

As we did in Section 3, we replicate and compare the same analysis with Wind measurements at 1 au. Because Wind's position is approximately fixed, it is not possible to reproduce the full joint pdf; but, below, we will show that the average occurrence rates at Wind are compatible with the PSP observations.

The average number of SBs per Mkm, as a function of the heliodistance, can be obtained from the joint distributions in Figure 3. Each column of the color plot represents the distribution of the number of SBs per Mkm at a fixed heliodistance. From each of these conditioned distributions $F(\nu, R^*)$, it is possible to obtain the average ν for each fixed R^*, computing the normalized first moment $\int d\nu' \nu' F(\nu', R^*) \Big/ \int d\nu' F(\nu', R^*)$. Each column's average value (or first moment) is displayed with a star-shaped symbol in Figure 3. The same treatment holds for Wind, except only one value of R^* is present. The above-obtained averages do not show any appreciable radial trend, as their values are almost constant within the variability from point to point.

From a certain perspective, the constancy of the SB rate may appear to be at odds with the systematic variation with distance of the other physical parameters. Taking such variations into account may introduce additional interesting physical interpretations. For example, we may consider the evolution of the turbulence correlation length. Comparison with estimated correlation lengths for each interval is not straightforward due to the relatively short interval duration we have adopted. The optimal interval size is $\gtrsim$15 hr (Isaacs et al. 2015). However, the general tendency of radial variation of correlation length can be reasonably estimated as $\lambda_C \sim 10^6\,\mathrm{km}\sqrt{R(\mathrm{au})}$ (Ruiz et al. 2014; M. E. Cuesta et al. 2022, in preparation).

Using this estimation, after a simple transformation, we arrive at Figure 4, which shows the average number of SBs per correlation length as a function of the radial distance. As a check, the same analysis has been performed by measuring the average number of SBs directly from the detected population,

rather than using the moments of the conditioned distributions, and the results (not shown) are indistinguishable.

The novel organization of the mean values, in Figure 4, points toward the following consideration: The average number of SBs per Mkm is constant, but the solar wind structure, in which they are embedded, is dynamically evolving. If we consider the correlation length to be the typical scale of turbulent eddies, the result that the average number of SBs per correlation length increases somehow allows that SBs can be also seen as a byproduct of turbulence, and their presence is enhanced as the turbulent cascade takes place.

5. Discussion of the Results and Conclusion

The topic of SBs in PSP observations has become very active due to the dramatic nature of these observations and the possible implications that these large magnetic field deflections may have for unraveling the physics of solar wind heating and acceleration (Bale et al. 2019; Kasper et al. 2019), which are central goals of the PSP mission. SB observations, particularly the radial variations of their occurrence and other properties studied by PSP, may be relevant to revealing the basic physics of the nascent solar wind.

The prolific appearance of SBs in PSP data sets has prompted investigators to analyze ensembles of identified cases to establish statistical properties and, therefore, in principle, a robust physical perspective. These studies have adopted varying definitions, leading to disparate identification criteria, thus emphasizing different physical properties. For example, the defining conditions in some studies do not require local polarity reversals, only angular deflections (Dudok de Wit et al. 2020). Other studies imply that high Alfvénicity should be a defining condition (Borovsky 2016; Horbury et al. 2018). Another approach is to identify source regions as a factor in the selection criteria (Tenerani et al. 2021). The approach employed here is intentionally simplified: We employ only the reversal of direction relative to a locally averaged field to be the sole fundamental condition for identifying an SB. As an a posteriori check, we examined our identified events to assess how many are likely to be associated with possible HCS crossings. For this purpose, we measured the average magnetic field component B_R, for PSP, and B_X, for Wind (respectively, in the RTN and GSE coordinate systems) 1 hour before the beginning of each SB, and 1 hour after its end. We define a potential HCS crossing when the two averages are of opposite sign and, in magnitude, larger than 5 (PSP) or 3 (Wind) nT (Burlaga & Ness 1968). We note that the rare circumstance in which PSP crosses the HCS and shortly thereafter crosses again, emerging on the original side, might not be recognized by this proxy and would be counted as SBs. The results indicate that such current sheet crossings represent ∼2% of the identified PSP events and ∼0.3% of the Wind events. Therefore, these cases do not have a substantial effect on the statistical descriptions we have provided.

There are of course subsidiary conditions that enter into the selection we have implemented. For example, as discussed in Section 2, the average magnetic field must be well-defined within the interval in question, and the appearance of too large a fraction of missing data points renders a particular time slice unusable. Our methodology, applied between 2018 August 12 and 2021 June 19 (∼1042 days), yielded a total of 22,223 SBs using PSP 10 s data and 6 hr averaging intervals. See Table 2 for a list including all configurations used in this study.

Table 2
Total Number of Switchbacks #SBs Identified with PSP and Wind, Varying the Magnetic Field Cadence Δt in Seconds and the Averaging Window width W in hours

Δt(s)	W(h)	#SBs (PSP)	#SBs (Wind)
10	3	19141	23793
10	6	22223	29908
60	3	6458	8117
60	6	7556	9301

We note that we included analyses only of data at heliocentric distances $r < 0.7$ au, even though some data were available in the range 0.7 au $< r < 1$ au. That range is excluded due to the relative scarcity of data. In part, this is due to the PSP orbit aphelia, which barely extend beyond 0.7 au after orbit 6, as well as lower data availability in general in that range (Chhiber et al. 2021).

On the threshold deflection angle. To further investigate the effects of our particular choice of the deflection angle that defines an SB (i.e., 90°), we performed the same analyses (not shown here) by also considering threshold angles of 60° and 120° between the local and the average magnetic fields. All of the cases show qualitatively the same results presented above. However, some dependence on the angle can be observed with regard to at least two key features: (I) The plateau reached after the sharp increase, for the 120° angle case, is reached much farther away, at about 0.3 au (compare with panels (b) and (e) of Figure 3), suggesting a local evolution, and (II) the average number of SBs per correlation length (shown here in Figure 4) monotonically decreases when increasing the angle, maintaining the same radial dependence. Note that the decrease in the frequency of occurrence with increasing fluctuation amplitude (deflection) is ordered in the same way as turbulent fluctuations are ordered—larger amplitudes occur less frequently. These results, building on existing literature (Mozer et al. 2020; Dudok de Wit et al. 2020), provide further evidence that SBs may be locally generated in the solar wind.

Characteristics of the observed SB rates. A salient feature of the SB occurrence rates seen in both Figures 3 and 4 is the appearance of a ramp at $r < 0.2$ au (i.e., $\sim 40\,R_\odot$). A naive extrapolation of this trend to zero SB rate occurs at around 20 solar radii. This is remarkably close to the radius at which the first passage into sub-Alfvénic coronal plasma was detected recently (Kasper et al. 2021; Chhiber et al. 2022). If one views this as an increase in SB rate beginning at ∼20 solar radii, then the "turning on" of SBs in this range of heliocentric distances appears to support the hypothesis that shear-driven activity is initiated in this vicinity. A proposed candidate is MHD mixing layer dynamics, leading to rollups of vorticity and magnetic field reversals (Ruffolo et al. 2020). This is also the same region in which the more-striated coronal plasma transitions to a more isotropic flocculated appearance in heliospheric imaging analyses (DeForest et al. 2016; Chhiber et al. 2019) of the inner solar wind.

Besides the Ruffolo et al. (2020) model, there are other models for the in situ generation of SBs (Squire et al. 2020; Schwadron & McComas 2021) that may also be consistent with the present observations. We also are not attempting here to garner evidence to controvert models for the generation of SBs at much lower altitudes, such as interchange reconnection in the chromosphere or lower corona (Fisk & Kasper 2020; Zank et al. 2020; Drake et al. 2021; Magyar et al. 2021a, 2021b). In

fact, there may be separate SB populations; some are generated at lower altitudes and experience attenuation (Tenerani et al. 2020) during propagation to radii beyond the Alfvén transition zone, while others are generated at higher altitudes (Tenerani et al. 2021) and will eventually experience attenuation at farther distances.

It is noteworthy that transforming the data from an SBs-per-kilometer format to an SBs-per-correlation scale format, as in Figure 4, does appear to produce a systematic ordering of the data. For example, the trends at low heliocentric distances of SBs/λ_c for both magnetic cadences approach a zero count rate near 0.1 au.

Meanwhile, the relatively smooth increase at larger R extrapolates reasonably well to the Wind results at 1 au. It is tempting to interpret this as support for the idea that turbulence properties are, at some level, controlling or influencing SB rates. However, it is difficult to assert that scaling to the correlation length is the only way to organize the data. As a matter of fact, the relatively flat plateau present at heliodistances greater than 0.2 au may allow various interpretations. The present choice of using the correlation length becomes appropriate when considering the scales at play. Indeed, the average duration of SBs falls within the scales of the inertial range of turbulence, making closer contact than other possible scales (e.g., the ion or electron skin depth).

Although the driving of the source in the lower solar atmosphere is definitely responsible for defining some of the macroscopic features of turbulence (Bale et al. 2021; Fargette et al. 2021; Magyar et al. 2021a, 2021b), given the systematic behavior of the SB rate seen in Figure 4, there is a strong suggestion that SB properties, including their rate of occurrence, are evolving and are controlled, at some level, by dynamics outside of about 0.1 au.

This research is partially supported by the Parker Solar Probe mission through the IS⊙IS Theory and Modeling team and a subcontract from Princeton University (SUB0000317), NASA PSP Guest Investigator grants 80NSSC21K1765 and 80NSSC21K1767, and NASA Heliospheric Supporting Research program grants 80NSSC18K1210 and 80NSSC18K1648. This project is also partially supported by the European Union's Horizon 2020 research and innovation program under grant agreement No. 776262 (AIDA, www.aida-space.eu). The PSP data used here are publicly available on NASA CDAWeb, https://cdaweb.gsfc.nasa.gov/index.html/. The authors thank the FIELDS team (PI: Stuart D. Bale, UC Berkeley), the Integrated Science Investigation of the Sun (IS⊙IS) Science Team (PI: David McComas, Princeton University), and the Solar Wind Electrons, Alphas, and Protons (SWEAP) team for providing data (PI: Justin Kasper, BWX Technologies). Parker Solar Probe was designed, built, and is now operated by the Johns Hopkins Applied Physics Laboratory as part of NASA's Living with a Star (LWS) program (contract NNN06AA01C). Support from the LWS management and technical team has played a critical role in the success of the Parker Solar Probe mission. F.P. thanks Mattia Rovito for his help with the design of the database webpage. L.P. thanks the ICT center of the University of Calabria for hosting the web server of the database.

Appendix
Online Database of Detected Switchbacks

The present work afforded an opportunity to assemble an open-access online catalog that accepts inquiries in the form of a specified time interval and provides a list of magnetic field reversals and the time of their occurrence. Assembly of such a database requires analyzing a large amount of raw data (months or years) from the public PSP archive folders.

The reproduction of such data can be achieved by replicating the download and analysis steps; this sacrifices quickness in favor of the economy of storage requirements. Another approach is to set up a capacious disk storing all possibly needed data sets to access them rapidly using a simple interface. The assembled database supports the latter approach for the convenience of the interested user.

The database is built using the parameters described in the paper. The user is asked to input the spacecraft (Wind or PSP), magnetic field cadence (10 s or 60 s), averaging window (3 hr or 6 hr), and a time interval (within the first eight orbits of PSP). The output is immediately provided as a list of UTC seconds, human-readable dates, and the value of z, for all the points that satisfy $z \geqslant 0.5$. The user can then choose to print the output on the screen or download it as a text file.

The database is freely accessible at http://astroplasmas.unical.it/SBDB/.

ORCID iDs

Francesco Pecora https://orcid.org/0000-0003-4168-590X
William H. Matthaeus https://orcid.org/0000-0001-7224-6024
Leonardo Primavera https://orcid.org/0000-0001-7004-789X
Antonella Greco https://orcid.org/0000-0001-5680-4487
Rohit Chhiber https://orcid.org/0000-0002-7174-6948
Riddhi Bandyopadhyay https://orcid.org/0000-0002-6962-0959
Sergio Servidio https://orcid.org/0000-0001-8184-2151

References

Bale, S. D., Badman, S. T., Bonnell, J. W., et al. 2019, Natur, 576, 237
Bale, S. D., Goetz, K., Harvey, P. R., et al. 2016, SSRv, 204, 49
Bale, S. D., Horbury, T. S., Velli, M., et al. 2021, ApJ, 923, 174
Bandyopadhyay, R., Matthaeus, W. H., Parashar, T. N., et al. 2020, ApJS, 246, 61
Bandyopadhyay, R., Matthaeus, W. H., McComas, D. J., et al. 2021, A&A, 650, L4
Borovsky, J. E. 2016, JGRA, 121, 5055
Burlaga, L. F., & Ness, N. F. 1968, CaJPh, 46, S962
Chhiber, R., Goldstein, M. L., Maruca, B. A., et al. 2020, ApJS, 246, 31
Chhiber, R., Matthaeus, W. H., Usmanov, A. V., Bandyopadhyay, R., & Goldstein, M. L. 2022, arXiv:2201.08422
Chhiber, R., Usmanov, A. V., Matthaeus, W. H., & Goldstein, M. L. 2019, ApJS, 241, 11
Chhiber, R., Usmanov, A. V., Matthaeus, W. H., & Goldstein, M. L. 2021, ApJ, 923, 89
Chhiber, R., Usmanov, A. V., Matthaeus, W. H., Parashar, T. N., & Goldstein, M. L. 2019, ApJS, 242, 12
DeForest, C. E., Matthaeus, W. H., Viall, N. M., & Cranmer, S. R. 2016, ApJ, 828, 66
Drake, J. F., Agapitov, O., Swisdak, M., et al. 2021, A&A, 650, A2
Dudok de Wit, T., Krasnoselskikh, V. V., Bale, S. D., et al. 2020, ApJS, 246, 39
Fargette, N., Lavraud, B., Rouillard, A. P., et al. 2021, ApJ, 919, 96

Farrell, W. M., MacDowall, R. J., Gruesbeck, J. R., Bale, S. D., & Kasper, J. C. 2020, ApJS, 249, 28
Fisk, L. A., & Kasper, J. C. 2020, ApJL, 894, L4
Fox, N. J., Velli, M. C., Bale, S. D., et al. 2016, SSRv, 204, 7
Horbury, T. S., Matteini, L., & Stansby, D. 2018, MNRAS, 478, 1980
Horbury, T. S., Woolley, T., Laker, R., et al. 2020, ApJS, 246, 45
Isaacs, J. J., Tessein, J. A., & Matthaeus, W. H. 2015, JGRA, 120, 868
Jokipii, J. R. 1973, ARA&A, 11, 1
Kasper, J. C., Abiad, R., Austin, G., et al. 2016, SSRv, 204, 131
Kasper, J. C., Bale, S. D., Belcher, J. W., et al. 2019, Natur, 576, 228
Kasper, J. C., Klein, K. G., Lichko, E., et al. 2021, PhRvL, 127, 255101
Laker, R., Horbury, T. S., Bale, S. D., et al. 2021, A&A, 650, A1
Landi, S., Hellinger, P., & Velli, M. 2006, GeoRL, 33, L14101
Lepping, R. P., Acũna, M. H., Burlaga, L. F., et al. 1995, SSRv, 71, 207
Liang, H., Zank, G. P., Nakanotani, M., & Zhao, L.-L. 2021, ApJ, 917, 110
Magyar, N., Utz, D., Erdélyi, R., & Nakariakov, V. M. 2021a, ApJ, 911, 75
Magyar, N., Utz, D., Erdélyi, R., & Nakariakov, V. M. 2021b, ApJ, 914, 8
Martinović, M. M., Klein, K. G., Huang, J., et al. 2021, ApJ, 912, 28
McCracken, K., & Ness, N. 1966, JGR, 71, 3315
McManus, M. D., Bowen, T. A., Mallet, A., et al. 2020, ApJS, 246, 67
Mozer, F. S., Agapitov, O. V., Bale, S. D., et al. 2020, ApJS, 246, 68
Mozer, F. S., Bale, S. D., Bonnell, J. W., et al. 2021, ApJ, 919, 60
Neugebauer, M., & Goldstein, B. E. 2013, in AIP Conf. Proc., 1539, SOLAR WIND 13: Proc. of the Thirteenth International Solar Wind Conference (New York: AIP), 46
Newman, M. 2005, ConPh, 46, 323
Ogilvie, K. W., Chornay, D. J., Fritzenreiter, R. J., et al. 1995, SSRv, 71, 55
Perez, J. C., Bourouaine, S., Chen, C. H. K., & Raouafi, N. E. 2021, A&A, 650, A22
Ruffolo, D., Matthaeus, W. H., Chhiber, R., et al. 2020, ApJ, 902, 94
Ruiz, M. E., Dasso, S., Matthaeus, W. H., & Weygand, J. M. 2014, SoPh, 289, 3917
Schwadron, N., & McComas, D. 2021, ApJ, 909, 95
Sioulas, N., Velli, M., Chhiber, R., et al. 2022, ApJ, 927, 140
Squire, J., Chandran, B. D. G., & Meyrand, R. 2020, ApJL, 891, L2
Tenerani, A., Sioulas, N., Matteini, L., et al. 2021, ApJL, 919, L31
Tenerani, A., Velli, M., Matteini, L., et al. 2020, ApJS, 246, 32
Zank, G. P., Nakanotani, M., Zhao, L.-L., Adhikari, L., & Kasper, J. 2020, ApJ, 903, 1